Journal of Food Engineering 369 (2024) 111918

Contents lists available at ScienceDirect

Journal of Food Engineering

journal homepage: www.elsevier.com/locate/jfoodeng

A starch digestion model considering intrinsic granular properties

Yifan Qin [a,b], Jie Xiao [b,**], Aibing Yu [a,c], Xiao Dong Chen [b,*]

[a] Department of Chemical Engineering and Biological Engineering, Monash University, Clayton, VIC, 3800, Australia
[b] School of Chemical and Environmental Engineering, College of Chemistry, Chemical Engineering and Materials Science, Soochow University, Suzhou, Jiangsu Province, 215123, China
[c] Southeast University-Monash University Joint Research Institute, Suzhou Industrial Park, Suzhou, Jiangsu Province, 215123, China

ARTICLE INFO

Keywords:
Mass transfer
Enzymatic reaction
Digestion
Particle shrinkage
Hydrolysis kinetics

ABSTRACT

Starch particle digestion is an important topic in food digestion research. This study has developed a diffusion-reaction model to characterize hindered enzyme diffusion and substrate hydrolysis on the surface and in the interior of porous starch particles. A moving boundary numerical method is applied to account for particle shrinkage caused by surface reaction. This model has been proven to predict the digestion rate of various starch particles of different sizes. The parameter estimation procedure quantifies the properties that are hard to measure by experimental techniques, i.e., diameter, reactive area, and proportion of pores accessible for enzyme as well as susceptibility of starch to enzyme. This work formulates a quantitative procedure for identifying the particle digestion pattern (i.e., outside-in or inside-out) by resorting to the developed model. Computational experiments indicate that in addition to internal architecture, particle size has a significant effect on the digestion pattern.

1. Introduction

Starch is the primary nutrient and energy source in our daily life. Its digestion in the gastrointestinal tract is a crucial rate-limited step of bioavailability to humans and is highly associated with human metabolism and health. Many modeling efforts have been devoted to understanding the digestive characteristics of different starchy foods. The most widely used is the first-order kinetics model, where the digestion rate is assumed to be in direct proportion to the substrate concentration, and the kinetics constant can reflect the relative susceptibility of starch to enzyme (Butterworth et al., 2011; Singh et al., 2010). Considering the substrate saturation effect, the Michaelis-Menten kinetics model has also been heavily applied when the substrate is in a large excess compared to the enzyme (van Boekel, 2008). Many research groups improved this model empirically in an attempt to consider more effects observed from digestion experiments, e.g., product inhibition (Dona et al., 2011). Despite these efforts, this empirical modeling approach currently takes a limited number of variables into account. It seems to be only feasible for the digestion of starch in liquid form, like a gelatinized solution, but invalid for granular starch digestion that involves a more complex mechanism.

The digestion of starch granules is a typical heterogeneous reaction. The factors limiting the rate of starch digestion can be broadly classified into two groups: catalyzed reaction related and mass transfer related. A critical factor influencing the digestion rate is the susceptibility of starch to the enzyme. At the molecular level, it is determined by the crystalline structures illustrated in Fig. 1(a). A polymorphic type with shorter double helices (found in most cereal starches) is more readily hydrolyzed compared to B polymorphic type with longer and more stable helices (found in most tuber starches) (Tester et al., 2004). From the perspective of mass transfer, both the rheological property of liquid phase and the architecture of solid phase profoundly influence the diffusion of molecules (Dhital et al., 2014; Grundy et al., 2016). Dhital et al. (2017) stated that the substantial presence of pores and channels allowed the enzyme easy access to regions inside the granule, which led to a specific digestion pattern known as the 'inside-out' pattern shown in Fig. 1(b). Conversely, the absence of pores and channels makes the enzyme penetrate the interior region slowly and hydrolyze granules primarily by surface erosion. It was described as 'outside-in' pattern. Identifying the digestion pattern can provide valuable guidance for food processing and modification. Nevertheless, it is unreasonable and less rigorous to determine the digestion pattern subjectively based on particle morphology. For an accurate evaluation, it is essential to quantitatively compare the amount of starch hydrolyzed on the particle surface

* Corresponding author.
** Corresponding author.
E-mail addresses: jie.xiao@suda.edu.cn (J. Xiao), xdchen@mail.suda.edu.cn (X.D. Chen).

https://doi.org/10.1016/j.jfoodeng.2023.111918
Received 6 October 2023; Received in revised form 22 December 2023; Accepted 25 December 2023
Available online 26 December 2023
0260-8774/

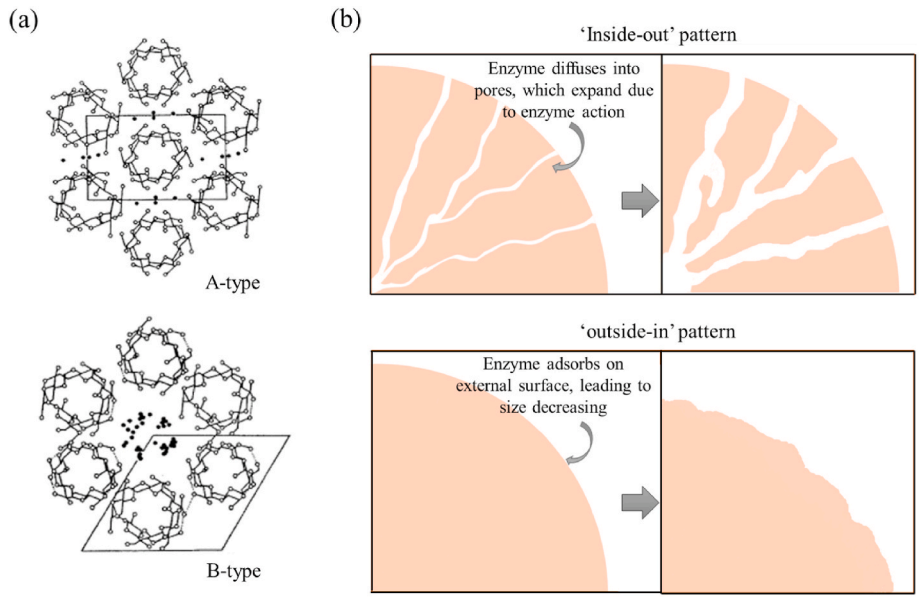

Fig. 1. The schematic diagram of (a) A-type and B-type crystal structures referred from Eliasson (2004), and (b) 'inside-out' and 'outside-in' digestion patterns (extreme cases drawn based on Dhital et al. (2017)).

and inside the particle.

To predict the rate and pattern of starch particle hydrolysis, a mechanism-driven model is required. It is a typical but unique diffusion-reaction problem. Unlike many traditional heterogeneous reactions like electrolysis (Kavand et al., 2021), the diffusing molecule in a digestion system is enzyme. It is not consumed but acts to promote the reaction rate. However, different from catalyst carriers in systems like fix-bed reactions (Park, 2018), starch particles undergo changes in both size and structure during hydrolysis. While previous investigations focused on the modeling of enzyme diffusion and substrate reactions, attention has primarily been paid to other substrates, such as protein (Sicard et al., 2018) and cellulose (Luterbacher et al., 2013). Moreover, all these models neglected the decrease in particle size during hydrolysis, which is exact evidence reported in digestion experiments (Chen et al., 2011; Tamura et al., 2016). Despite posing a challenge for numerical solving, incorporating the dynamic changes in both size and structure into the modeling is crucial for a more accurate prediction of the starch particle digestion process.

This work will propose a diffusion-reaction model for the in-vitro digestion of starch particles featured as size shrinking and architecture evolution. The following section details basic assumptions, mathematical equations, and numerical methods. In-vitro digestion experiments are referred to evaluate the model and estimate the initial parameters that are hard to measure by experimental methods, e.g., the initial proportion of pores accessible to the enzyme. Meanwhile, a quantitative procedure for identifying the digestion pattern of different starches is formulated based on the developed model, which can help offer more efficient guidelines for food processing. It should be pointed out that this strategy may also hold promise for enhancing the reaction efficiency in other fields, e.g., biorefinery (Raj et al., 2022) and electrolysis (Kavand et al., 2021). Beyond understanding digestion mechanisms, this mechanistic model has the potential to be integrated with existing intestinal models (Qin et al., 2023), providing insight into in-vivo digestion phenomena that are challenging to observe experimentally. Furthermore, its application is anticipated in improving glycemic prediction systems (Oviedo et al., 2017), enabling the consideration of food properties and the calculation of the glycemic index (GI) (Goñi et al., 1997).

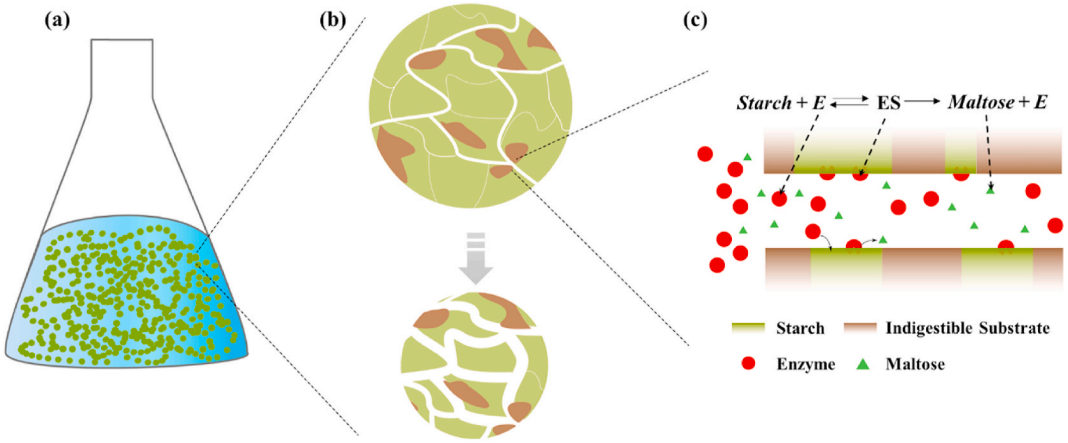

Fig. 2. Multiscale illustration of the hydrolysis of starchy particles in an in-vitro digestion experiment. (a) The macroscopic view of a digestion experiment. (b) The changes in particle size and pore geometry before and after digestion. (c) The enzymatic reaction in a nanopore.

2. Model development

2.1. Model description and assumption

Starch particles hydrolyzed in an in-vitro system are modeled as completely dispersed spheres with identical physicochemical properties as shown in Fig. 2(a). This basic assumption aligns with the general modelling practice for hydrolysis of particles with uncertain shape, e.g., protein (Sicard et al., 2018) and cellulose (Movagharnejad and Sohrabi, 2003). Generally, in-vitro digestion experiments involve three successive steps, i.e., oral, gastric, and intestinal phases, to imitate a complete digestive journey. For the digestion of starch, the roles of the former two steps (oral and gastric) are negligible in consideration of the short reaction duration of the oral phase (about 10~20 s) and rapid inactivation of α-amylase in the acidic environment of the gastric phase (van Boekel, 2008; Al-Rabadi et al., 2009; Tamura et al., 2016). The simulation initiates at the beginning of the intestinal stage. The concentration of α-amylase in the intestinal simulated fluid is estimated by summing the amounts of α-amylase and water added throughout all three phases. The pH value, which influences the enzyme activity, remains steady in that the neutral reaction of acid and base completes rapidly at the beginning of the intestinal phase. The product resulting from α-amylase hydrolysis is exclusively assumed to be maltose because the variety of oligosaccharides is too complex.

In the microscale view depicted in Fig. 2(b), numerous pores of varying diameters are distributed inside a particle containing digestible starch and indigestible components, e.g., fibers, protein, lipid, etc. These minor ingredients may contribute to diverse granular structures and varying impacts on the digestion process, but the underlying mechanisms are too intricate to establish precise mathematical relationships. As a first approximation, they are all considered as enzyme-resistant substrates with identical properties. As the hydrolysis occurs, the granule size gradually decreases as starch and other indigestible components are dissociated into the surrounding solution. Simultaneously, the internal pores expand, accompanied by the shrinkage of the solid phase where the starch content declines but the region of other components is unchanged. Consequently, the diffusivity of solute and available surface area both change accordingly. Notably, not all the pores estimated by experimental methods, e.g., nitrogen adsorption (Juszczak et al., 2002), are larger than the size of α-amylase. Pores too narrow to allow α-amylase to enter are considered inaccessible regions in this simulation. Due to the destructive role of acid and pepsin on the granular structure during the gastric phase, the information on pores at the beginning of the intestinal phase is unknown. Moreover, different from materials in other disciplines, the nature of a certain food varies from one experiment to another due to different origins or processing methods (Ho et al., 2013). Initial values of pore-related parameters are unavailable and need to be estimated. Fig. 2(c) gives a conceptive illustration of how the enzyme dissociates starch from the solid-liquid interface of pores. It is assumed that the adsorption and desorption of enzymes have no influence on the localized enzyme concentration in pores.

2.2. Mathematical equations

2.2.1. Diffusion of enzyme

Driven by the concentration difference, the enzyme in the external aqueous solution migrates toward the core of a porous particle. The mass balance of the enzyme can be described by Fick's second law:

$$\frac{\partial E}{\partial t}=\frac{1}{r^2}\frac{\partial}{\partial r}\left(r^2 D_{E,p}\frac{\partial E}{\partial r}\right) \tag{1}$$

where E [U/m^3] denotes the enzyme concentration at time t at the radial distance r from the core of a particle. $D_{E,p}$ [m^2/s] is the effective diffusivity of the enzyme in a porous structure. U is an international unit of enzyme catalytic activity, and 1 U is the amount of enzyme that catalyzes the conversion of 1 μmol of substrate per minute. Under the premise of constant temperature and pH, the ability to convert the substrate is directly proportional to the enzyme amount, so U/m^3 can be regarded as a concentration unit. The initial condition of Eq. (1) is

$$E|_{t=0}=0 \tag{2}$$

The Neumann boundary condition imposed on the partial differential equation at the particle surface is given by:

$$D_{E,l}\frac{\partial E}{\partial r}\Big|_{r=R_p}=k_l(E_l-E_s) \tag{3}$$

Here E_l and E_s are the enzyme concentration in the surrounding environment and on the particle surface, respectively. The environmental concentration is assumed to be a constant. That is the decline of enzyme concentration due to diffusing into particles is negligible, given that the external space is significantly larger than the pore volume in particles, and the enzyme is not consumed by reaction. $D_{E,l}$ [m^2/s] is the diffusivity of the enzyme in the external aqueous solution. The mass transfer coefficient, denoted as k_l, characterizes the mass exchange at the boundary of a particle. It is estimated based on the correlation of the solid-liquid mass transfer in an agitated system derived from the previous literature (Wojtusik et al., 2016).

$$Sh=0.69Re^{0.5}Sc^{1/3} \tag{4}$$

The Sherwood, Reynolds and Schmidt dimensionless numbers are related to the flow conditions around particles by Eqs. (5)–(7)

$$Sh=\frac{k_l d_p}{D_{E,l}} \tag{5}$$

$$Re=\frac{Nd_T^2\rho_l}{\mu} \tag{6}$$

$$Sc=\frac{\mu}{\rho_l D_{E,l}} \tag{7}$$

Here d_p [m] denotes the particle diameter, which decreases as a result of the hydrolysis taking place on the outer surface. N [s^{-1}] is the stirring speed, and d_T [m] is the vessel diameter. ρ_l [kg/m^3] and μ [Pa s] are the density and viscosity of the liquid media, respectively. The diffusivity in the external aqueous solution $D_{E,l}$ can be calculated by the Einstein-Stokes equation:

$$D_{E,l}=\frac{k_B T}{3\pi\mu d_E} \tag{8}$$

where k_B is the Boltzmann constant, T is the absolute temperature (310 K), and d_E [m] is the hydrodynamic diameter of the enzyme. In addition, the enzyme diffusion inside a porous particle is affected by pore-related properties. The following equation gives the effective diffusivity of the enzyme in a porous structure $D_{E,p}$ [m^2/s].

$$D_{E,p}=\frac{\varepsilon}{\tau}D_{E,pore} \tag{9}$$

where ε denotes the localized porosity. It increases as the hydrolysis reaction consumes the localized solid component, and it can be expressed as a function related to the mass of the solid component per unit particle volume X [kg/m^3].

$$\varepsilon=1-(1-\varepsilon_0)\frac{X}{X_0} \tag{10}$$

Here ε_0 and X_0 are respectively the initial values of the corresponding variables.

The tortuosity factor τ in Eq. (9) is given by an empirical correlation of ε for porous media (Weissberg, 1963):

$$\tau = 1 - 0.5 \ln \varepsilon \tag{11}$$

The molecular size of the enzyme is comparable to the average diameter of pores. Its migration inside a particle is hindered by the presence of the pore wall (Fournier, 2017). The diffusivity $D_{E,pore}$, which describes the hindered diffusion in solvent-filled pores, is reduced by two factors. Its general form can be expressed as

$$D_{E,pore} = D_{E,l} F_1(\varphi) F_2(\varphi) \tag{12}$$

The correction factors F_1 and F_2 in Eq. (12) are both functions of φ, which is the ratio of the enzyme diameter d_E to the pore diameter d_{pore}:

$$\varphi = \frac{d_E}{d_{pore}} \tag{13}$$

In the current work, only the pores more extensive than the enzyme are considered so that there is no case of $\varphi > 1$. Given the assumption of cylindrical pore geometry (see Fig. 2(c)), the change in pore diameter exhibits a square-root relationship with the change in pore volume.

$$d_{pore} = d_{pore,0} \sqrt{\frac{\varepsilon}{\varepsilon_0}} \tag{14}$$

where $d_{pore,0}$ is the initial pore diameter. Real particles exhibit a broad distribution of pore diameter. Given the extreme challenge of acquiring the distribution along the radial direction, this study employs the same initial value at each position, specifically the average. The first hindrance to diffusion is known as steric exclusion. It implies that a solute cannot approach the pore wall closer than its radius, thus limiting the pore cross-sectional area available to a solute. The correction factor F_1, namely the stearic partition coefficient, is defined as follows:

$$F_1 = (1 - \varphi)^2 \tag{15}$$

Diffusion in a pore comparable in size to the solute is also restricted by increased hydrodynamic drag. Regarding the hydrodynamic hindrance factor F_2, the widely-used empirical equation developed by Dechadilok and Deen (2006) is employed:

$$F_2(\varphi) = 1 - 2.104\varphi + 2.09\varphi^3 - 0.95\varphi^5 \tag{16}$$

2.2.2. Enzyme catalysis of starch

The enzymatic reaction in a starchy particle involves two steps, adsorption and catalysis, as depicted in Fig. 2(c). The adsorption of the enzyme on the solid-liquid interface can be described by the interfacial Langmuir equilibrium isotherm (van Boekel, 2008):

$$q = \frac{E^*_{max} E}{K_m + E} \tag{17}$$

where E^*_{max} [U/m^2] represents the saturation interfacial concentration of enzyme and K_m [U/m^3] is the equilibrium constant. The rate of the formation of the final product per unit area [kg/(m^2·s)] is given by

$$\frac{k_{cat} E^*_{max} E}{K_m + E} = \frac{V_{max} E}{K_m + E} \tag{18}$$

where k_{cat} [s^{-1}] is the kinetic rate constant of product formation. The product of k_{cat} and E^*_{max} is defined as V_{max} [kg/(m^2·s)], which represents the maximum rate of product formation per unit area.

To describe the reaction occurring inside a particle, the interfacial reaction rate needs to be transformed into a volumetric rate, which is equal to the decreasing rate of the solid component:

$$\frac{\partial X}{\partial t} = -\frac{V_{max} E A_i (1 - \eta)}{K_m + E} \tag{19}$$

The initial condition of Eq. (19) is

$$X|_{t=0} = X_0 \tag{20}$$

It implies that a raw particle has the same density at every position. However, different enzymatic hydrolysis rate between the inner and outer regions of the particle leads to a time-dependent distribution of density along the radial direction. The solid component is composed of digestible starch and indigestible substrate.

$$X = X_{dig} + X_{indig} \tag{21}$$

The available area for the enzymatic reaction inside a particle depends on the area of the solid-liquid interface A_i and the digestible ratio $(1 - \eta)$ (see the green region in Fig. 2(c)). The interfacial area per unit particle volume A_i [m^2/m^3] is computed based on the assumption of cylindrical pores (detailed derivation is provided in Appendix A)

$$A_i = A_{i,0} \sqrt{\frac{\varepsilon}{\varepsilon_0}} \tag{22}$$

If one assumes that starch and other components resistant to α-amylase possess the same density, the fraction of the indigestible component is a function of the solid mass per unit particle volume:

$$\eta = \frac{X_{indig}}{X} = \frac{X_{indig,0}}{X_0} \frac{X_0}{X} = \eta_0 \frac{X_0}{X} \tag{23}$$

The rate of starch production from a particle is the sum of the internal rate and surface rate.

$$Q_{sum} = Q_i + Q_s \tag{24}$$

Integrating Eq (19) gives the rate of starch hydrolysis inside a particle:

$$Q_i = \int_0^{R_p} 4\pi r^2 \frac{V_{max} E A_i (1 - \eta)}{K_m + E} dr \tag{25}$$

The rate of starch hydrolyzed on the external surface of a particle can be directly obtained based on the enzyme concentration on the particle surface:

$$Q_s = \frac{V_{max} E_s A_p (1 - \eta_s)}{K_m + E_s} \tag{26}$$

where A_p [m^2] denotes the available external surface area of a particle, which declines as a result of particle shrinking, and η_s is the fraction of indigestible components on the surface. Considering the pores and indigestible component on the particle boundary, the computation of A_p is given by:

$$A_p = 4\pi {R_p}^2 (1 - \varepsilon_s) \tag{27}$$

where ε_s is the porosity on the particle surface. As the enzymatic reaction proceeds, particles shrink accomplished by the dissociation of starch and the indigestible component from the external surface. According to Appendix B, the decreasing rate of the particle radius on the premise of $\eta_s \neq 1$:

$$\frac{\partial R_p}{\partial t} = -\frac{V_{max} E_s (1 - \varepsilon_0)}{(K_m + E_s) X_0} \tag{28}$$

When the digestible component on the surface is exhausted, that is $\eta_s = 1$, the shrinking of a particle ceases. The internal reaction generates a reduction in the starch content inside a particle. The average mass of starch per unit granular volume can be calculated by its spatial distribution:

$$\overline{X}_{dig} = \frac{3 \int_0^{R_p} r^2 X_{dig} dr}{R_p^3} \tag{29}$$

To better compare the influences of surface reaction and internal reaction on a particle, the extents of change in particle size and starch proportion are characterized by $R_p/R_{p,0}$ and $\overline{X}_{dig}/X_{dig,0}$, respectively. $R_{p,0}$ and $X_{dig,0}$ are their initial values.

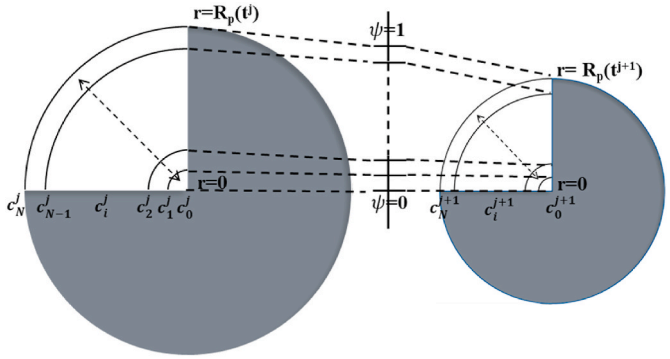

Fig. 3. The Landau transformation introduces new positional variables of which the interval is [0, 1]. A fixed discretization of these variables corresponds to points whose position varies in real space to accommodate the motion of the external boundary.

2.3. Numerical method

In this model, the decrease in the particle radius leads to a moving boundary problem, also known as the Stefan problem (Illingworth and Golosnoy, 2005; Zhang and White, 2007). The Landau transformation, a moving boundary solving method, has been successfully implemented in both the diffusion equation Eq. (1) and the reaction equation Eq. (19) to achieve greater precision. It constructs an adaptive scheme that relocates a constant number of nodes by moving the mesh points and keeps a node located at the boundary.

This method introduces a new positional variable $\psi = r/R_p$, as shown in Fig. 3, to fix the physical domain $0 \le r \le R_p$ to the computational domain $0 \le \psi \le 1$. The governing equation Eq. (1) is rewritten in terms of ψ:

Table 1
Parameter values used in the model with references.

Experiment	Parameter	Value	References
Native sorghum	X_0	1.37 g/cm^3	McDonough et al. (2004)
	η_0	34.3% ~43%	Al-Rabadi et al. (2009)
	E_l	1157 U/ml	Al-Rabadi et al. (2009)
Native barley	X_0	1.2 g/cm^3	Hoyle et al. (2019)
	η_0	48.3% ~71.4%	Al-Rabadi et al. (2009)
	E_l	1157 U/ml	Al-Rabadi et al. (2009)
Native maize	X_0	1.23 g/cm^3	Bhise et al. (2014)
	η_0	33 %	Liu et al. (2016)
	E_l	58 U/ml	Dhital et al. (2010)
Native potato	X_0	1.35 g/cm^3	Adane et al. (2006)
	η_0	30 %	Liu et al. (2007)
	E_l	58 U/ml	Dhital et al. (2010)
Cooked rice	X_0	0.9 g/cm^3	Le and Jittanit (2012)
	η_0	22.8 %	Ranawana et al. (2010)
	E_l	37 U/ml	Ranawana et al. (2010)
Common parameters	d_E	7 nm	Payan et al. (1980)
	d_T	5 cm	*
	N	85 rpm	(Dhital et al., 2010; Al-Rabadi et al., 2009)
	T	310 K	
	μ	0.001 Pa s	*

*values are estimated from general knowledge.

$$\frac{\partial E}{\partial t} - \frac{\psi}{R_p}\frac{dR_p}{dt}\frac{\partial E}{\partial \psi} = \frac{1}{(\psi R_p)^2}\frac{\partial}{\partial \psi}\left(D_{E,p}\psi^2\frac{\partial E}{\partial \psi}\right) \tag{30}$$

The boundary condition:

$$D_{E,l}\left.\frac{\partial E}{\partial \psi}\right|_{\psi=1} = k_l(E_l - E_s) \tag{31}$$

$$\left.\frac{\partial E}{\partial \psi}\right|_{\psi=0} = 0 \tag{32}$$

The equation Eq. (19) can be transformed to the following form:

$$\frac{\partial X}{\partial t} - \frac{\psi}{R_p}\frac{dR_p}{dt}\frac{\partial X}{\partial \psi} = -\frac{V_{max}EA_i(1-\eta)}{K_m + E} \tag{33}$$

The initial conditions of the above equations do not require any transformation. While the introduction of the Landau transformation complicates the governing equations, it simplifies the problem by keeping the computational domain fixed instead of changing with time. The diffusion-reaction model in the form of Landau transformation is solved with spatial discretization along the r coordinate by the central finite difference method (see Fig. 3) and the temporal discretization by the forward Euler method. The equations were solved numerically in MATLAB.

2.4. Parameter estimation method

To quantitatively compare the simulation results with in-vitro experiments, a commonly used metric, namely hydrolysis ratio, is computed by Eq. (34). It represents the mass of starch hydrolyzed divided by the initial mass of starch in a particle:

$$H = \frac{6\int_0^t Q_{sum}dt}{\pi d_{p,0}^3 X_0(1-\eta_0)} \tag{34}$$

The parameter estimation is carried out using the developed model against experimental data from previous literature. The objective function of the regression problem is

$$\min \sum_{m=1}^{M}\sum_{n=1}^{N}\left(H_{exp}^{m,n} - H_{sim}^{m,n}\right)^2 \tag{35}$$

where M is the number of the experimental groups, and N is the number of the sampling time points in the experiment. The subscripts *sim* and *exp* represent simulation data and experimental data, respectively.

The goodness of fit R^2 will be used to evaluate the effectiveness of model parameters for different particle sizes.

$$R^2 = 1 - \frac{SSE}{SST} \tag{36}$$

where SSE is the residual sum of squares, and SST is the total sum of squares. The value of R^2 approaching 1 indicates a better agreement between the simulated and experimental results.

$$SSE = \sum_{n=1}^{N}\left(H_{exp}^{n} - H_{sim}^{n}\right)^2 \tag{37}$$

and

$$SST = \sum_{n=1}^{N}\left(H_{exp}^{n} - \overline{H_{exp}}\right)^2 \tag{38}$$

2.5. Identification of digestion pattern

A rigorous criterion for the digestion pattern of starch particles can be formulated with the aid of the developed model. The idea is to estimate and compare the amount of starch hydrolyzed in the interior and

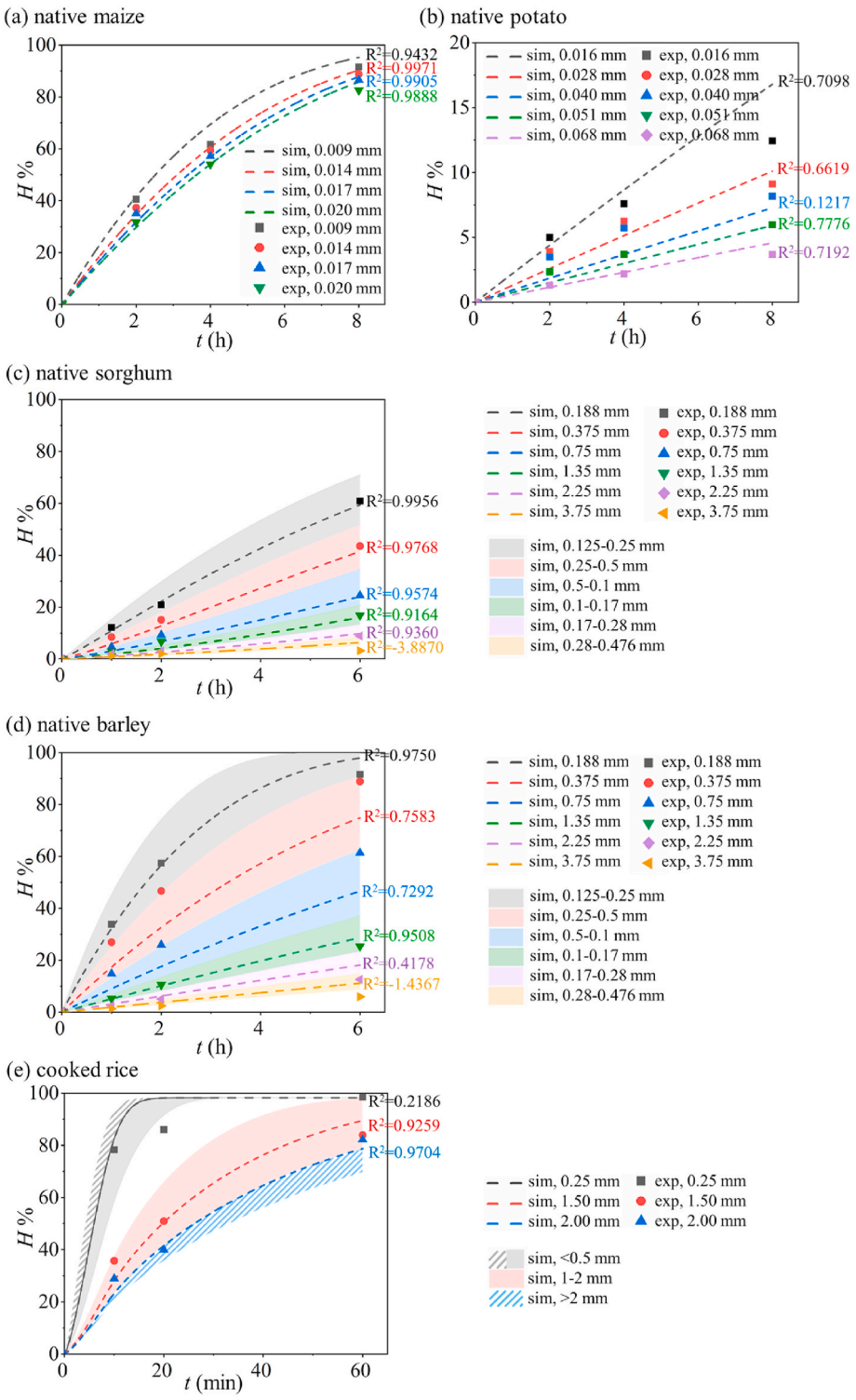

Fig. 4. Model fitting results of hydrolysis ratio for five starchy foods (native maize, native potato, native sorghum, native barley, and cooked rice) with different initial particle sizes as well as R2 value for each size group. Dots: in-vitro experimental data. Lines: simulation results by average particle size. Patterns: uncertainty of simulation results (stripes denote borderless).

on the surface in a certain period of time. Based on the reaction rates obtained from Eq. 24–26, the percentages of internal reaction and surface reaction within time t can be quantified, respectively.

$$P_i = \frac{\int_0^t Q_i dt}{\int_0^t Q_{sum} dt} \times 100\% \tag{38}$$

$$P_s = \frac{\int_0^t Q_s dt}{\int_0^t Q_{sum} dt} \times 100\% \tag{39}$$

In this work, the period of time is set to 6 h. If the surface reaction contributes more than the internal reaction, that is $P_i|_{t=6\ h}$ >50%, the digestion pattern is defined as “inside-out”. Otherwise, the pattern is “outside-in”.

Table 2
Optimal parameter values for the model.

	V_{max} [kg/(m^2·s)]	K_m [U/ml]	ε_0	$A_{i,0}$ [m^2/m^3]	$d_{pore,0}$ [nm]
Maize	1.42×10^{-6}	600	0.29	2.3×10^5	14
Potato	6.65×10^{-7}	1529	0.192	2×10^4	14.2
Sorghum	2.32×10^{-6}	1123	0.185	1.65×10^4	13.1
Barley	4.8×10^{-6}	200	0.084	5.98×10^2	25
Rice	1.32×10^{-5}	1.1	0.48	1.39×10^5	13.7

3. Results & discussion

3.1. Parameter identification

Three digestion experiments (Al-Rabadi et al., 2009; Dhital et al., 2010; Ranawana et al., 2010) focusing on the effects of particle size on the hydrolysis rate of five starchy foods (i.e., maize, potato, sorghum, barley, and cooked rice) were selected to validate the effectiveness of the model. The particle size in different experiments varied significantly, ensuring that the proposed model can be verified for general applicability. The experimental conditions of these studies and the available properties of different starchy foods are given in Table 1. The enzyme concentrations in the surrounding solution were estimated by considering the total amount of α-amylase and the total volume of water added throughout the entire hydrolysis process. The initial ratios of indigestible content of sorghum and barley were provided explicitly in the original paper. However, the indigestible content was not directly measured in the experiments involving maize, potato, and rice. Rough estimations were made based on information from other references to approximate this parameter for these starchy foods.

The fitting profiles for the hydrolysis ratio of the selected foods against time, as well as the corresponding in-vitro experimental data, are presented in Fig. 4. The values of R^2 indicate the prediction fidelity for each particle size group. The parameter estimation results are summarized in Table 2. In Fig. 4(a, c & e), the data for maize, sorghum and cooked rice demonstrate a satisfactory fit to the proposed model. In comparison, the results of potato and barley in Fig. (b & d) exhibit a moderate level of accuracy. The biases for most groups are within an acceptable range for a biochemical reaction (Ozili, 2023). It can be found that the fitting goodness is notably low for sorghum and barley with the largest particle size (3.75 mm). This discrepancy may stem from the relatively intact cell wall and a more continuous protein network before grilling (Dhital et al., 2017), which has been neglected in the current work. Hence, it can be roughly summarized that the estimated parameters are applicable within a size range of approximately 0.1–2 mm for sorghum, barley and cooked rice, and 0.01–0.1 mm for maize and potato.

Apart from the inherent complexity of the digestive process, these errors could be attributed to the uncertainty in particle size. In in-vitro digestion experiments, researchers used starch particles with a large size distribution instead of a completely uniform size. While the experiments for maize and potato accurately measured the average particle diameters using a reliable method, i.e., surface weighted mean, the rough estimates of the average size based on sieving range for sorghum, barley and rice might not offer precise predictions. Therefore, the deviation of simulation results in consideration of the uncertainty of the average particle size is depicted in Fig. 4(c, d & e), revealing that the vast majority of experimental dots fall within the corresponding region.

3.2. Digestion behavior analysis

Apart from the excellent performance in calculating the hydrolysis rate of various starch-rich particles of different sizes, the estimated parameters in Table 2 *can help shed light on the underlying mechanisms that determine the gap in digestion behavior. The susceptibility of starch to amylase, reflected by the parameter* V_{max}, is influenced by factors such as the ratio of amylose to amylopectin, the length of branch chains of amylopectin, crystalline structure, and the packing of amorphous phases (Dhital et al., 2017). In the case of cooked rice, this parameter is much higher compared to native starches, indicating that it is susceptible to α-amylase. This is because heating in excess water disrupts the crystalline structure of rice starch, which consequently makes it readily available for enzymatic attack (Singh et al., 2010). Furthermore, cooking causes the swelling of granules and the leakage of components, resulting in a more open granular network (Jang et al., 2016). This is evident by the top initial values of porosity and the available inner area of cooked rice. The estimated porosity (0.48) is within the range (0.25–0.5) observed in experimental research (Ramesh, 2000).

Among the investigated native starches, barley has a relatively higher value of V_{max}. It implies that the stronger enzyme sensitivity is the dominating reason for the more rapid hydrolysis of barley particles, which possess lower porosity and smaller effective internal area. Similar evidence can also be found in the experimental research that compared the amylolysis behavior between barley and maize (Naguleswaran et al., 2013). Despite more pores on the surface of maize particles observed by SEM images, barley particles were hydrolyzed to a greater extent due to their weaker crystalline structure, which was confirmed by wide angle X-ray diffraction (WAXD). Potato, a representative tuber starch with B-type polymorph, shows a lower value of V_{max}, aligning with experimental observations. The hexagonal packing of helices formed by amylopectin with longer chains in B-type crystals imparts greater stability to the internal structure, making it more resistant to breakdown (Butterworth et al., 2011).

The initial values of internal surface area $A_{i,0}$ and porosity ε_0 of maize particles are much higher than those of other native starches. More interestingly, even though potato is often perceived as lacking pores, its values of $A_{i,0}$ and ε_0 approach the magnitude of sorghum. This intriguing trend could be explained by the micrometer-scale grain size used in the maize and potato digestion experiments (Dhital et al., 2010). Individual endosperm cells typically range from 50 to 150 μm, so starch in granules of millimeter-scale size is predominately encapsulated by intact cell walls. In contrast, granules of micrometer-level size contain more broken cells, providing additional exposed sites for enzyme binding and catalysis reaction. Industrial processing techniques such as milling are also likely to destroy crystalline regions and protein networks, further increasing opening channels and available reactive area (Dhital et al., 2017). In addition, a common phenomenon can be found further by comparing the values of $A_{i,0}$ obtained from the same experiment (i.e., sorghum vs. barley and maize vs. potato). It indicates that the larger internal area leads to a slighter disparity in digestion kinetics among different size groups in that the increase in $A_{i,0}$ impairs the influence brought by the change in the external surface area.

3.3. Comparison of digestion pattern

This section compares the contributions of surface reaction and internal reaction to determine the digestion pattern of different starch particles. The initial particle size for each variety was set within the applicable range estimated in the previous section. Fig. 5(a1∼e1) show the relative contributions of internal reaction and surface reaction to the total hydrolysis. The decreased degree of particle size and average starch content, given by Eqs. (28) and (29), are plotted in Fig. 5(a2∼e2). The evolution of effective diffusivity within a particle is drawn in Fig. 5 (a3∼e3).

As hydrolysis proceeds, all groups demonstrate a consistent tread, characterized by a decrease in the surface reaction ratio and an increase in the internal reaction ratio. This can be ascribed to two changes involved. One is the declining outer surface area, which occurs due to the decrease in the particle size. The other change is the enhancement of enzyme concentration inside the particle, particularly during the initial

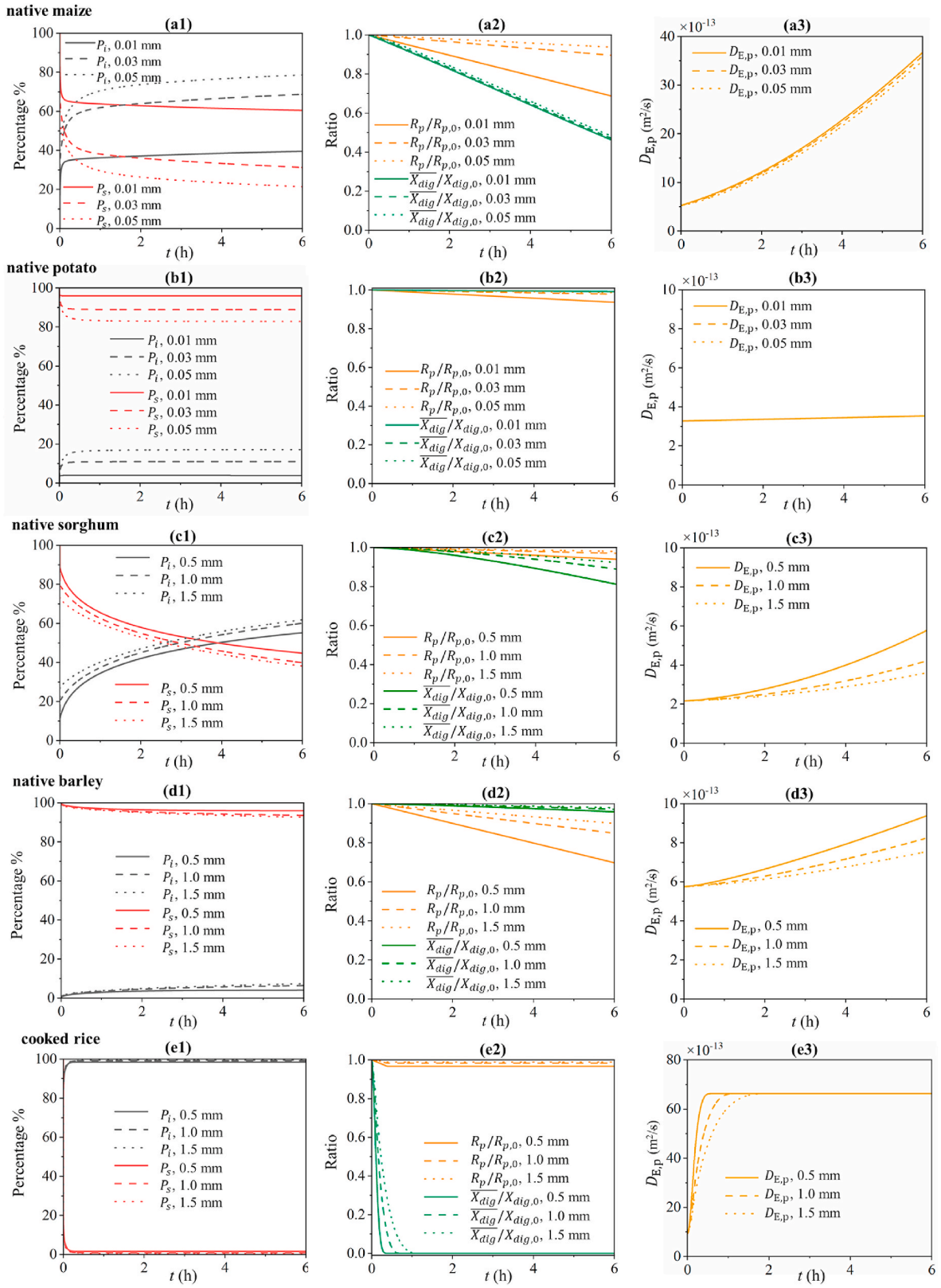

Fig. 5. The effect of initial particle size on the digestion behavior of five starches. P_i & P_s: percentages of internal and surface reactions; $R_p/R_{p,0}$ & $\overline{X_{dig}}/X_{dig,0}$: degrees of change in particle size and starch proportion; $D_{E,p}$: effective diffusivity.

period. The second common tendency can be observed when comparing profiles of different initial sizes. As the initial diameter increases, the surface reactive contribution decreases, and the internal reactive contribution experiences the opposite. According to the spherical area and volume formulas, the specific surface area of a particle is inversely proportional to its radius (i.e., $3/R_p$), indicating that a pile of particles with smaller average size has a larger total external surface area. Additionally, as shown in Fig. 5(a2~e2) & (a3~e3), smaller particles experience relatively more dramatic changes in particle size, starch content and effective diffusivity.

From the left subgraphs of Fig. 5, one can see a vast disparity in the digestion pattern among different starchy foods. According to the classification defined in the methodology part, maize granules with initial average size of 0.01 mm are digested by "outside-in" pattern (surface reaction making up about 60%), while the other two size groups behave the opposite. The size-dependent pattern is owing to the higher proportion of outer surface area in finer grains compared to coarser grains (referring to the inverse relationship between the outer surface area per unit granular volume and the radius). It is stated that starch particles of the same component but different sizes are likely to be digested in different patterns. In Fig. 5(c1), the hydrolysis ratios of all three sorghum groups in the interior surpass those on the outer surface after approximately 3 h, and ultimately reach about 60% at 6 h. The digestion behavior of sorghum within the given particle size range can be described as an "inside-out" pattern. As listed in Table 2, sorghum possesses more accessible pores for the enzyme to enter the hilum region and more inner area that provides more catalysis sites, so the erosion by enzyme in the interior plays a dominant role in the whole process. The contributions of surface reaction for potato and barley, as shown in Fig. 5(b1 & d1), are in an absolutely dominant position (over 90%) throughout the period. Their digestion patterns are hence classified as "outside-in".

Fig. 5(e1) suggests that cooked rice, which is highly susceptible to enzymatic action and has extensive pores, undergoes nearly complete consumption by internal reaction. As illustrated in Fig. 5(e2), the starch located within the interior is exhausted in a very short time, and the granular radius experiences a slight reduction only at the very beginning. In an in-vitro rice digestion experiment conducted by Tamura et al. (2016), the ultimate digestion reached nearly 90%, and the average size of grains also went through two changes, i.e., decreasing rapidly in the very early stage and remaining almost constant in the later stage.

Distinct structural variations in grains with different digestion patterns are observable in the middle subgraphs of Fig. 5. Generally, starch particles digested by the "outside-in" pattern (e.g., barley and potato) undergo a more remarkable change in particle size compared to starch proportion. Conversely, the "inside-out" pattern (e.g., sorghum and rice) contributes to an opposite trend. Furthermore, one can see a universal relationship between the middle and right subgraphs. The extent of increase in effective diffusivity is positively correlated with the extent of starch consumption in the granular interior. It implies that the internal hydrolysis reaction can create a more porous structure, thereby enhancing mass transfer behavior.

4. Conclusion

This study developed a starch particle hydrolysis model that considered evolutions of particle size and internal structure. The accuracy of the model was verified by published experimental data. Moreover, the generic model has been used to investigate various starch particles of different sizes. This work addressed the challenge of estimating initial parameters that cannot be directly measured experimentally. These estimated parameters uncover the in-depth mechanisms that influence the digestion behavior. However, it is essential to note that the estimated parameters have limited applicability, ranging from approximately 0.1 to 2 mm for sorghum, barley, and cooked rice, and from 0.01 to 0.1 mm for maize and potato. Unlike conventional starch digestion models, e.g., 1st kinetics function, this mechanistic model is able to adapt changes in the external environment, paving the way for predicting digestion behavior in the gastrointestinal tract with complex physiological features.

A rigorous and efficient strategy to distinguish the digestion pattern is presented in this study. In addition to internal structure, particle size plays a crucial role in determining the digestion pattern. The quantitative method, based on mathematical modeling, can offer high-efficiency approaches for food processing or modification. For instance, to slow down the hydrolysis rate of "outside-in" particles like barley, more attention should be paid to controlling the surface reaction, which can be achieved by selecting coarse grains. For "inside-out" particles, diffusion inhibition measures, such as adding soluble dietary fibers to increase fluid viscosity, would be more practical.

Symbols

A_i	Effective internal surface area per unit particle volume [m^2/m^3]
A_p	Effective external surface area of a particle [m^2]
d_E	Hydrodynamic diameter of enzyme [m]
d_p	Particle diameter [m]
d_{pore}	Pore diameter [m]

CRediT authorship contribution statement

Yifan Qin: Writing - original draft, Validation, Software, Methodology, Formal analysis, Data curation. **Jie Xiao:** Writing - review & editing, Supervision, Project administration, Methodology, Formal analysis, Conceptualization. **Aibing Yu:** Supervision, Funding acquisition, Conceptualization. **Xiao Dong Chen:** Writing - review & editing, Supervision, Project administration, Funding acquisition, Formal analysis, Conceptualization.

Declaration of competing interest

The authors declare that they have no known competing financial interests or personal relationships that could have appeared to influence the work reported in this paper.

Data availability

Data will be made available on request.

Acknowledgements

The authors are grateful for the financial support from the National Natural Science Foundation of China (21978184 & 22078212). Prof. Jie Xiao acknowledges the "Jiangsu Innovation and Entrepreneurship (Shuang Chuang) Program" and the "Jiangsu Specially-Appointed Professors Program".

d_T	Vessel diameter [m]
$D_{E,l}$	Diffusivity of enzyme in the surrounding environment [m^2/s]
$D_{E,pore}$	Diffusivity of enzyme in hindered pores [m^2/s]
$D_{E,p}$	Effective diffusivity of enzyme within a particle [m^2/s]
E	Enzyme concentration within a particle [U/m^3]
E_l	Enzyme concentration in the surrounding environment [U/m^3]
E_s	Enzyme concentration on the particle surface [U/m^3]
E^*_{max}	Saturation concentration of enzyme on the solid-liquid interface [U/m^3]
F_1	Correction factor of φ [−]
F_2	Correction factor of φ [−]
H	Hydrolysis ratio [−]
k_{cat}	Rate constant of product formation [kg/(U·s)]
k_B	Boltzmann constant [−]
K_m	Equilibrium constant [U/m^3]
N	Stirring speed [s^{-1}]
P_i	Percentage of internal reaction [%]
P_s	Percentage of surface reaction [%]
q	Adsorption amount of enzyme on the solid-liquid interface [U/m^2]
Q_i	Rate of starch hydrolysis in the interior of a particle [kg/s]
Q_s	Rate of starch hydrolysis on the surface of a particle [kg/s]
Q_{sum}	Total hydrolysis rate of a particle [kg/s]
r	Radial distance to the core of a particle [m]
R_p	Particle radius [m]
T	Absolute temperature [K]
t	Time [s]
V_{max}	Maximum rate of product formation per unit area [kg/(m^2·s)]
X	Solid mass per unit particle volume [kg/m^3]
X_0	Initial value of X [kg/m^3]
X_{dig}	Digestible solid mass per unit particle volume [kg/m^3]
X_{indig}	Indigestible solid mass per unit particle volume [kg/m^3]
ε	Porosity [−]
ε_0	Initial value of ε [−]
ε_s	Value of ε on the particle surface [−]
τ	Tortuosity factor [−]
ψ	A new positional variable equal to r/R_p [−]
μ	Viscosity [Pa·s]
η	Ratio of indigestible components [−]
ρ_l	Liquid density [kg/m^3]

Appendix A

Based on the assumption of cylindrical pores, the surface area per unit pore volume can be expressed as:

$$A_{pore} = \frac{4\pi d_{pore} l}{\pi d_{pore}^2 l} = \frac{4}{d_{pore}} \tag{A.1}$$

thus obtaining $A_{pore} \propto {}^{1}/_{d_{pore}}$, and it gets

$$\frac{A_{pore}}{A_{pore,0}} = \frac{d_{pore,0}}{d_{pore}} \tag{A.2}$$

Referring to Eq. (14),

$$A_{pore} = A_{pore,0}\sqrt{\frac{\varepsilon_0}{\varepsilon}} \tag{A.3}$$

and then substituting it into $A_i = \varepsilon A_{pore}$ yields:

$$A_i = \varepsilon \frac{A_{i,0}}{\varepsilon_0}\sqrt{\frac{\varepsilon_0}{\varepsilon}} = A_{i,0}\sqrt{\frac{\varepsilon}{\varepsilon_0}} \tag{A.4}$$

Appendix B

The decreasing rate of the volume of a particle is equal to the rate of surface reaction divided by the mass of digestible solid per unit volume on the surface:

$$\frac{\partial V_p}{\partial t} = -\frac{V_{max} E_s A_p (1-\eta_s)}{(K_m + E_s)(1-\eta_s) X_s} \tag{B.1}$$

The premise of the equation above is $\eta_s \neq 1$. Referring to the expression of the effective external surface area Eq. (27), it can be rewritten:

$$\frac{\partial V_p}{\partial t} = -\frac{4\pi {R_p}^2 V_{max} E_s (1-\varepsilon_s)}{(K_m + E_s) X_s} \tag{B.2}$$

According to Eq. (10),

$$\frac{\partial V_p}{\partial t} = -\frac{4\pi {R_p}^2 V_{max} E_s \left(1-\varepsilon_{s,0}\right)}{(K_m + E_s) X_{s,0}} \tag{B.3}$$

The rule of partial derivation gives that

$$\frac{\partial V_p}{\partial t} = \frac{\partial \frac{4}{3}\pi {R_p}^3}{dt} = 4\pi {R_p}^2 \frac{\partial R_p}{\partial t} \tag{B.4}$$

According to Eq. (B.3) and Eq. (B.4), it gets the rate of the change of particle radius

$$\frac{\partial R_p}{\partial t} = -\frac{V_{max} E_s \left(1-\varepsilon_{s,0}\right)}{(K_m + E_s) X_{s,0}} = -\frac{V_{max} E_s (1-\varepsilon_0)}{(K_m + E_s) X_0} \tag{B.5}$$

References

Adane, M., Endale, A., Bultosa, G., Abdel-Mohsen, M.G., Gebre-Mariam, T., 2006. Isolation and physicochemical characterization of Godare (Colocasia esculenta) starch from Ethiopia. Ethiop. Pharm. J. 24 (1), 13–22.

Al-Rabadi, G.J., Gilbert, R.G., Gidley, M.J., 2009. Effect of particle size on kinetics of starch digestion in milled barley and sorghum grains by porcine alpha-amylase. J. Cereal. Sci. 50 (2), 198–204.

Bhise, S., Kaur, A., Manikantan, M., 2014. Moisture dependent physical properties of maize (PMH-1). Acta Aliment. 43 (3), 394–401.

Butterworth, P.J., Warren, F.J., Ellis, P.R., 2011. Human α-amylase and starch digestion: an interesting marriage. Starch-Stärke. 63 (7), 395–405.

Chen, J., Gaikwad, V., Holmes, M., Murray, B., Povey, M., Wang, Y., Zhang, Y., 2011. Development of a simple model device for in vitro gastric digestion investigation. Food Funct. 2 (3–4), 174–182.

Dechadilok, P., Deen, W.M., 2006. Hindrance factors for diffusion and convection in pores. Ind. Eng. Chem. Res. 45 (21), 6953–6959.

Dhital, S., Shrestha, A.K., Gidley, M.J., 2010. Relationship between granule size and in vitro digestibility of maize and potato starches. Carbohydr. Polym. 82 (2), 480–488.

Dhital, S., Dolan, G., Stokes, J.R., Gidley, M.J., 2014. Enzymatic hydrolysis of starch in the presence of cereal soluble fibre polysaccharides. Food Funct. 5 (3), 579–586.

Dhital, S., Warren, F.J., Butterworth, P.J., Ellis, P.R., Gidley, M.J., 2017. Mechanisms of starch digestion by α-amylase—structural basis for kinetic properties. Crit. Rev. Food Sci. Nutr. 57 (5), 875–892.

Dona, A.C., Pages, G., Gilbert, R.G., Kuchel, P.W., 2011. Starch granule characterization by kinetic analysis of their stages during enzymic hydrolysis: 1H nuclear magnetic resonance studies. Carbohydr. Polym. 83 (4), 1775–1786.

Eliasson, A.C., 2004. Starch in Food: Structure, Function and Applications. CRC press, New York.

Fournier, R.L., 2017. Basic Transport Phenomena in Biomedical Engineering. CRC press, New York.

Goñi, I., Garcia-Alonso, A., Saura-Calixto, F., 1997. A starch hydrolysis procedure to estimate glycemic index. Nutr. Res. 17 (3), 427–437.

Grundy, M.M., Edwards, C.H., Mackie, A.R., Gidley, M.J., Butterworth, P.J., Ellis, P.R., 2016. Re-evaluation of the mechanisms of dietary fibre and implications for macronutrient bioaccessibility, digestion and postprandial metabolism. Br. J. Nutr. 116 (5), 816–833.

Ho, Q.T., Carmeliet, J., Datta, A.K., Defraeye, T., Delele, M.A., Herremans, E., Opara, L., Ramon, H., Tijskens, E., van der Sman, R., Liedekerke, P.V., Verboven, P., Nicolaï, B. M., 2013. Multiscale modeling in food engineering. J. Food Eng. 114 (3), 279–291.

Hoyle, A., Brennan, M., Jackson, G.E., Hoad, S., 2019. Increased grain density of spring barley (Hordeum vulgare L.) is associated with an increase in grain nitrogen. J. Cereal. Sci. 89, 102797.

Illingworth, T., Golosnoy, I., 2005. Numerical solutions of diffusion-controlled moving boundary problems which conserve solute. J. Comput. Phys. 209 (1), 207–225.

Jang, A., Kim, J.Y., Lee, S., 2016. Rheological, thermal conductivity, and microscopic studies on porous-structured noodles for shortened cooking time. Lwt 74, 1–6.

Juszczak, L., Fortuna, T., Wodnicka, K., 2002. Characteristics of cereal starch granules surface using nitrogen adsorption. J. Food Eng. 54 (2), 103–110.

Kavand, M., Mollaabbasi, R., Ziegler, D., Larachi, F., Picard, D., Alamdari, H., 2021. Reaction-diffusion model for gasification of a shrinking single carbon-anode particle. ACS Omega 6 (12), 8002–8015.

Le, T.Q., Jittanit, W., 2012. Drying characteristics of cooked jasmine brown rice and true densities of dried products. Agric. Nat. Resour. 46 (2), 256–271.

Liu, N., Xue, Y., Guo, Z., Li, W., Tang, J., 2016. Genome-wide association study identifies candidate genes for starch content regulation in maize kernels. Front. Plant Sci. 7, 1046.

Liu, Q., Tarn, R., Lynch, D., Skjodt, N.M., 2007. Physicochemical properties of dry matter and starch from potatoes grown in Canada. Food Chem. 105 (3), 897–907.

Luterbacher, J.S., Parlange, J.Y., Walker, L.P., 2013. A pore-hindered diffusion and reaction model can help explain the importance of pore size distribution in enzymatic hydrolysis of biomass. Biotechnol. Bioeng. 110 (1), 127–136.

McDonough, C., Floyd, C., Waniska, R., Rooney, L., 2004. Effect of accelerated aging on maize, sorghum, and sorghum meal. J. Cereal. Sci. 39 (3), 351–361.

Movagharnejad, K., Sohrabi, M., 2003. A model for the rate of enzymatic hydrolysis of some cellulosic waste materials in heterogeneous solid–liquid systems. Biochem. Eng. J. 14 (1), 1–8.

Naguleswaran, S., Vasanthan, T., Hoover, R., Bressler, D., 2013. The susceptibility of large and small granules of waxy, normal and high-amylose genotypes of barley and corn starches toward amylolysis at sub-gelatinization temperatures. Food Res. Int. 51 (2), 771–782.

Ozili, P.K., 2023. The acceptable R-Square in empirical modelling for social science research. In: Saliya CA. Social Research Methodology and Publishing Results: A Guide to Non-native English Speakers. IGI Global, pp. 134–143.

Oviedo, S., Vehí, J., Calm, R., Armengol, J., 2017. A review of personalized blood glucose prediction strategies for T1DM patients. Int. J Numer. Meth. Bio. 33 (6), e2833.

Park, H.M., 2018. A multiscale modeling of fixed bed catalytic reactors. Int. J. Heat Mass Tran. 116, 520–531.

Payan, F., Haser, R., Pierrot, M., Frey, M., Astier, J.P., Abadie, B., Duée, B., Buisson, G., 1980. The three-dimensional structure of α-amylase from porcine pancreas at 5 Å resolution–the active-site location. Acta. Crystallogr. Sect. B-Struct. Sci. Cryst. Eng. Mat. 36 (2), 416–421.

Qin, Y., Chen, X.D., Yu, A., Xiao, J., 2023. New understanding from intestinal absorption model: how physiological features influence mass transfer and absorption. AIChE J. 69 (8), e18099.

Raj, T., Chandrasekhar, K., Kumar, A.N., Banu, J.R., Yoon, J.J., Bhatia, S.K., Yang, Y.H., Varjani, S., Kim, S.H., 2022. Recent advances in commercial biorefineries for lignocellulosic ethanol production: current status, challenges and future perspectives. Bioresource Technol 344, 126292.

Ramesh, M., 2000. Effect of cooking and drying on the thermal conductivity of rice. Int. J. Food Prop. 3 (1), 77–92.

Ranawana, V., Monro, J.A., Mishra, S., Henry, C.J., 2010. Degree of particle size breakdown during mastication may be a possible cause of interindividual glycemic variability. Nutr. Res. 30, 246–254.

Sicard, J., Mirade, P.S., Portanguen, S., Clerjon, S., Kondjoyan, A., 2018. Simulation of the gastric digestion of proteins of meat bolus using a reaction-diffusion model. Food Funct. 9 (12), 6455–6469.

Singh, J., Dartois, A., Kaur, L., 2010. Starch digestibility in food matrix: a review. Trends Food Sci. Technol. 21 (4), 168–180.

Tamura, M., Singh, J., Kaur, L., Ogawa, Y., 2016. Impact of structural characteristics on starch digestibility of cooked rice. Food Chem. 191, 91–97.

Tester, R.F., Karkalas, J., Qi, X., 2004. Starch structure and digestibility enzyme-substrate relationship. World Poultry Sci. J. 60 (2), 186–195.

van Boekel, M.A., 2008. Kinetic Modeling of Reactions in Foods. CRC press, New York.

Weissberg, H.L., 1963. Effective diffusion coefficient in porous media. J. Appl. Phys. 34 (9), 2636–2639.

Wojtusik, M., Zurita, M., Villar, J.C., Ladero, M., Garcia-Ochoa, F., 2016. Influence of fluid dynamic conditions on enzymatic hydrolysis of lignocellulosic biomass: effect of mass transfer rate. Bioresour. Technol. 216, 28–35.

Zhang, Q., White, R.E., 2007. Moving boundary model for the discharge of a LiCoO[sub 2]. Electrode. J. Electrochem. Soc. 154 (6), A587.